ACADEMIC PRESS

Available online at www.sciencedirect.com
SCIENCE DIRECT®

Journal of Sound and Vibration 265 (2003) 61–79

JOURNAL OF SOUND AND VIBRATION

www.elsevier.com/locate/jsvi

Spatial filters in structural control

A. Preumont*, A. François, P. De Man, V. Piefort

Active Structures Laboratory, Université Libre de Bruxelles, CP. 165/42, 50 Av. F.D. Roosevelt, B-1050 Brussels, Belgium

Received 21 August 2001; accepted 2 July 2002

Abstract

This paper discusses the use of modal filters in structural control. Discrete piezoelectric array sensors are first discussed and their lack of roll-off due to spatial aliasing is pointed out. In the second part, a new porous distributed electrode concept is introduced, which allows the effective piezoelectric coefficient to be tailored in two dimensions.

1. Introduction

There are two broad ways to achieve spatial filtering: (i) arrays of discrete sensors and (ii) continuous distributed sensors. Discrete sensor arrays may include accelerometers, strain gauges, piezoelectric patches, etc., while continuous distributed sensors may consist of piezoelectric films or optical fibres (the latter will not be considered in this study). The output of a piezoelectric sensor is a weighted average of the surface strains in the region covered by the electrodes on the film.

Modal filtering was initially proposed as an alternative to state observers to reduce spillover in modal control [1]. Discrete modal filters can be constructed from the orthogonality conditions of the mode shapes; they can also be constructed from modal test data [2–4]. Discrete piezoelectric array sensors have been considered as modal sensors for beams [5] or as volume velocity sensor for plates [6]. Discrete array sensors, if wired with independent conditioning electronics, are reconfigurable, but they suffer from spatial aliasing when sensing structural modes with wavelengths comparable to the spacing between sensors in the array. Although successful

*Corresponding author.
E-mail address: andre.preumont@ulb.ac.be (A. Preumont).

0022-460X/03/$ - see front matter
doi:10.1016/S0022-460X(02)01440-2

applications of modal control with discrete modal point sensors and actuators have indeed been reported (e.g. Refs. [3,4]), spatial aliasing usually brings major limitations for applications in structural control, as illustrated later in this paper (a good rule of thumb regarding sensor selection is that the quality of the sensor must in general be guaranteed one decade above the bandwidth of the control system).

When a distributed sensor is located in the far field, that is, far from the actuator and from the structural boundaries and singularities, the sensor output can be viewed as the filtered output of a point sensor at the centre of the distributed sensor [7]; the sensor's dynamics are obtained directly from the Fourier transform of the spatial distribution of the sensor. This allows the design of distributed sensors with specified low-pass filtering properties featuring high order roll-off without phase lag (with an apparent violation of the Bode's gain-phase relationships). However, in structural control, it is often advantageous to locate the actuator and sensor as close as possible to each other, to produce an interlacing pattern of poles and zeros (such a pattern is strictly achieved for collocated actuator/sensor pairs, but it can still be achieved in low frequency if the actuator and sensor are reasonably close, e.g. Ref. [8]). Unfortunately, in this case, the farfield condition is violated and the interpretation of the spatial sensor becomes more difficult.

The modal filtering of one-dimensional structures with continuous PVDF films can be traced to Refs. [9–11]. It is achieved by tailoring the width of the electrode (and possibly reversing the polarity). Although the spatial filtering of plates and shells with two-dimensional PVDF films has been suggested [11], it has never been implemented for lack of capability of continuously shaping the piezoelectric properties of the sensor material. One method of turning round this difficulty by a proper electrode design is discussed in this paper.

The use of orthogonal unidirectional PVDF films for spatial filtering of two-dimensional structures has been investigated in Refs. [12–14]; applications of multiple one-dimensional PVDF films to sound radiation sensing has been proposed in Refs. [15,16]. Multiple piezoelectric film sensors have been considered by Kim et al. and Miller et al. [17,18].

This review is by no means exhaustive, and we apologize for many omissions, but it gives an impression of the amount of research effort devoted to this field by the smart structures community. The objective of this paper is to explain the difficulties related to the spatial aliasing that were met in attempting to use discrete piezoelectric array sensors in feedback control loops, and to describe the original electrode design that the authors have developed to solve these problems. The paper is organized as follows. The first part examines the construction of modal filters from an array of discrete piezoelectric patches connected to a linear combiner; the linear combiner coefficients are calculated from a model of the structure, or from experimental FRFs. The tailoring of the open-loop FRF in a frequency band through proper selection of the linear combiner coefficients is also addressed. Next, an experiment is conducted; it confirms the good tailoring at low frequency, but reveals strong departures from the ideal behaviour at higher frequencies, due to spatial aliasing. The spatial aliasing is further analyzed numerically on the test configuration with arrays of increasing sizes. The second part of the paper examines the corresponding distributed sensor as a limit discrete array sensor when the number of sensing elements increases to infinity. A new electrode concept is then introduced, which allows the effective piezoelectric coefficients to be tailored in two dimensions; the electrode design is validated by 3-D finite element calculations and tests.

2. Modal filtering with an array sensor

2.1. From a known model of the structure

It is first assumed that there is an accurate linear model of a known structure. The modal expansion of the FRF of the sensor array reads

$$Y_k(\omega) = \sum_{i=1}^{m} \frac{c_{ki} b_i}{\mu_i(\omega_i^2 - \omega^2 + 2j\xi_i\omega_i\omega)}, \quad k = 1, \ldots, n, \tag{1}$$

where b_i is the modal input gain (at the actuator) and c_{ki} is the modal output gain of sensor k in the array.

If the n sensors in the array are connected to a linear combiner with gain α_k for sensor k (Fig. 1), the output of the linear combiner is $y = \sum_{k=1}^{n} \alpha_k y_k$ and the global frequency response is

$$G(\omega) = \sum_{k=1}^{n} \alpha_k Y_k(\omega) = \sum_{i=1}^{m} \frac{\{\sum_{k=1}^{n} \alpha_k c_{ki}\} b_i}{\mu_i(\omega_i^2 - \omega^2 + 2j\xi_i\omega_i\omega)}. \tag{2}$$

A modal filter which isolates mode l can be constructed by selecting the weighting coefficients α_k of the linear combiner in such a way that

$$\sum_{k=1}^{n} \alpha_k c_{ki}(\omega) = \delta_{li} \tag{3}$$

or

$$\boldsymbol{\alpha}^{\mathrm{T}} \mathbf{C} = \mathbf{e}_l^{\mathrm{T}} \tag{4}$$

where $\boldsymbol{\alpha} = (\alpha_1 \ldots \alpha_n)^{\mathrm{T}}$ is the vector of the linear combiner coefficients, $\mathbf{C} = c_{ki}$ is the matrix of modal output gain (column i is the sensor array output when the structure vibrates according to mode i) and $\mathbf{e}_l = (0\ 0 \ldots 1 \ldots 0)^{\mathrm{T}}$ is the vector with all entries equal to 0 except entry l which is equal to 1. Assuming that matrix $\mathbf{C}$ is known accurately, the modal filter coefficients $\boldsymbol{\alpha}_l$ for mode l can be found by solving the rectangular system of equations

$$\mathbf{C}^{\mathrm{T}} \boldsymbol{\alpha}_l = \mathbf{e}_l. \tag{5}$$

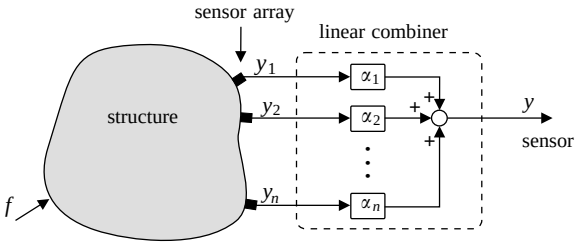

Fig. 1. Representation of the modal filter using n discrete sensors.

The number of columns of $\mathbf{C}^{\mathrm{T}}$, n, is equal to the number of sensors in the array and the number of lines, m, is equal to the number of modes included in the truncated modal expansion (1). The solution of Eq. (5) is discussed next section.

If the set of weighting coefficients $\boldsymbol{\alpha}_l$ satisfy Eq. (4), the open-loop FRF of the system, Eq. (2), becomes

$$G(\omega) = \frac{b_l}{\mu_l(\omega_l^2 - \omega^2 + 2\mathrm{j}\xi_l\omega_l\omega)}. \tag{6}$$

Its maximum value is obtained at $\omega = \omega_l$; it is equal to [19]

$$\|G(\omega)\|_\infty = \frac{b_l}{2\mu_l\xi_l\omega_l^2}. \tag{7}$$

2.2. *Modal filter coefficients* $\boldsymbol{\alpha}_l$

The solution of Eq. (5) requires some care because of the rank deficiency of $\mathbf{C}$ connected to the spatial aliasing. In fact, if the column of $\mathbf{C}$ (that is the modal contributions of the array sensor) are independent, the rank r of $\mathbf{C}$ follows the continuous line in Fig. 2: $r = m$ as long as $m \leqslant n$ and $r = n$ thereafter. This is the case, for example, for a simply supported beam with a regular array sensor, or for a simply supported square plate with a square array sensor. However, it is easy to check that for a *rectangular* plate with a uniform array sensor, the columns of $\mathbf{C}$ are not independent, resulting in a rank deficiency as indicated in dotted line in Fig. 2. (The spatial aliasing is illustrated in Fig. 9 which shows two columns of $\mathbf{C}$, corresponding, respectively, to mode (1,1) (mode # 1) and mode (1,15) (mode # 69).) Similarly, mode (1,9) (# 24) will be aliased into mode (1,7) (# 14). Spatial aliasing will be discussed further later in this paper.

The difficulty associated with the rank deficiency of $\mathbf{C}$ can be overcome by using a singular value decomposition of $\mathbf{C}^{\mathrm{T}}$ [20].

$$\mathbf{C}^{\mathrm{T}} = \mathbf{U}_1\boldsymbol{\Sigma}\mathbf{U}_2^H, \tag{8}$$

where $\mathbf{U}_1$ and $\mathbf{U}_2$ are unitary matrices containing the eigenvectors of $\mathbf{C}^{\mathrm{T}}\mathbf{C}$ and $\mathbf{C}\mathbf{C}^{\mathrm{T}}$, respectively, and $\boldsymbol{\Sigma}$ is the rectangular matrix of dimension (m, n) with the singular values σ_i on the diagonal (the superscript H is used to indicate the Hermitian). If $\mathbf{u}_i$ are the column vectors of $\mathbf{U}_1$ and $\mathbf{v}_i$ the

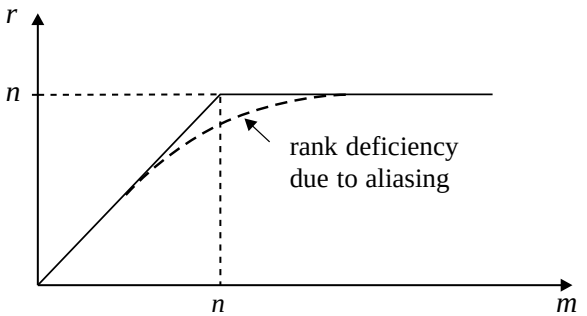

Fig. 2. Rank r of $C(m, n)$ as a function of the number of modes m in the modal expansion (1).

column vectors of $\mathbf{U}_2$, Eq. (8) can be written

$$\mathbf{C}^{\mathrm{T}} = \sum_{i=1}^{r} \sigma_i \mathbf{u}_i \mathbf{v}_i^H \tag{9}$$

and the solution of Eq. (5) reads

$$\boldsymbol{\alpha}_l = (\mathbf{C}^{\mathrm{T}})^{+} \mathbf{e}_l, \tag{10}$$

where the pseudo-inverse reads

$$(\mathbf{C}^{\mathrm{T}})^{+} = \sum_{i=1}^{r} \frac{1}{\sigma_i} \mathbf{v}_i \mathbf{u}_i^H. \tag{11}$$

This equation shows that the lowest singular values tend to dominate the pseudo-inverse, which is the origin of the problem in solving Eq. (5). In practice, however, the columns of $\mathbf{C}$ are not strictly proportional and its exact rank is not always easy to determine. The problem can be solved by truncating all the singular values below some tolerance value. In general, the solution is easier to achieve when the modal truncation is such that $m<n$.

2.3. Tailoring the open-loop FRF with the array sensor

Let $\boldsymbol{\alpha}_l$ be the set of the linear combiner weighting coefficients leading to modal filters. If the modes are well separated and if the damping is low, it is possible to find a set of weighting coefficients of the array sensor such that the open-loop FRF features the following properties:

1. The poles and zeros alternate near the imaginary axis (interlacing).
2. The peaks of the FRF at the resonances have a prescribed amplitudes A_i (Fig. 3).

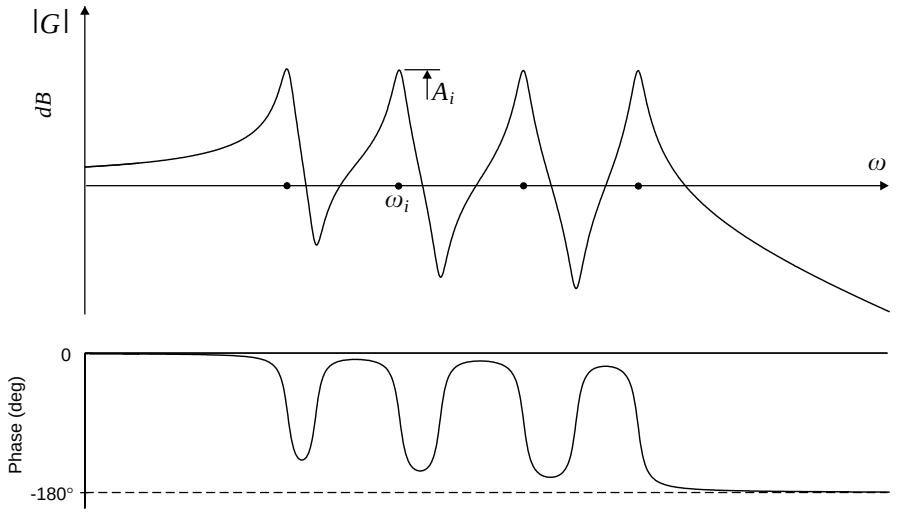

Fig. 3. Construction of a FRF with resonance peaks of prescribed amplitudes A_i and alternating poles and zeros.

The weighting coefficients can be obtained as follows: if the damping is low and the modes are well separated, the magnitude at a resonance peak is dominated by the contribution of the corresponding mode. Eq. (7) gives the maximum amplitude achieved with the linear combiner coefficients $\boldsymbol{\alpha}_l$. It follows that if the coefficients are taken as $w_l\boldsymbol{\alpha}_l$ with

$$w_l = \frac{2\mu_l\xi_l\omega_l^2}{b_l}A_l \tag{12}$$

the maximum amplitude of the response will be exactly A_l ($A_l > 0$). Since, for low damping and well separated modes, the amplitude at resonance is dominated by the contribution of the resonant mode, it follows that the set of weighting coefficients:

$$\boldsymbol{\alpha} = \sum_{l=1}^{M} w_l\boldsymbol{\alpha}_l \tag{13}$$

will lead to an open-loop FRF with a set of fixed amplitudes A_l at the resonances of the M selected modes [19]. Besides, if Eqs. (12) and (13) are substituted into Eq. (2), the FRF reads

$$G(\omega) = \sum_{i=1}^{M} \frac{2\xi_i\omega_i^2 A_i}{(\omega_i^2 - \omega^2 + 2\mathrm{j}\xi_i\omega_i\omega)}. \tag{14}$$

Since all the residues are positive, alternating poles and zeros are guaranteed [21].

2.4. From experimental data

The following problem is now addressed. The individual FRF $Y_k(\omega)$ of the n sensors in the array have been measured and the natural frequency ω_i and the modal damping ξ_i of one mode have been determined (with a modal analysis software). What are the weighting coefficients α_k of the linear combiner leading to a modal filter within some bandwidth $[\omega_a, \omega_b]$ and with unit amplitude at resonance (Fig. 4)

$$G_i(\omega) = \frac{2\xi_i\omega_i^2}{(\omega_i^2 - \omega^2 + 2\mathrm{j}\xi_i\omega_i\omega)}. \tag{15}$$

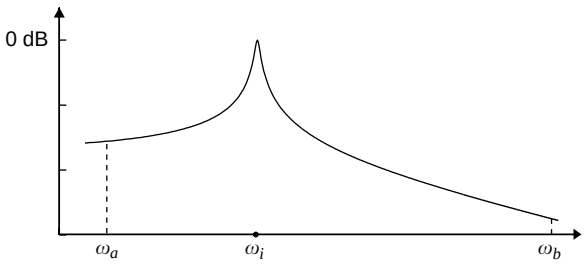

Fig. 4. Perfect modal filter within the bandwidth $[\omega_a, \omega_b]$ and with unit amplitude at ω_i.

The output FRF of the linear combiner reads

$$G(\omega) = \sum_{k=1}^{n} \alpha_k Y_k(\omega) \tag{16}$$

and the weighting coefficients α_k satisfy

$$\sum_{k=1}^{n} \alpha_k Y_k(\omega) = G_i(\omega). \tag{17}$$

If this equation is written at a set of p discrete frequencies v_i ($p > n$) regularly distributed over the frequency band $[\omega_a, \omega_b]$ the function equality (17) can be transformed into a redundant system of linear equations:

$$\begin{pmatrix} Y_1(v_1) & \dots & Y_n(v_1) \\ Y_1(v_2) & \dots & Y_n(v_2) \\ & \vdots & \\ Y_1(v_p) & \cdots & Y_n(v_p) \end{pmatrix} \begin{pmatrix} \alpha_1 \\ \alpha_2 \\ \vdots \\ \alpha_n \end{pmatrix} = \begin{pmatrix} G_i(v_1) \\ G_i(v_2) \\ \vdots \\ G_i(v_p) \end{pmatrix} \tag{18}$$

or, in matrix form,

$$\mathbf{Y}\boldsymbol{\alpha} = \mathbf{G}_i, \tag{19}$$

where the rectangular matrix $\mathbf{Y}$, of dimension (p, n), and the vector $\mathbf{G}_i$ are complex quantities and the vector $\boldsymbol{\alpha}$ of the linear combiner coefficients is real.

The solution of this redundant system of linear equations was addressed in Ref. [6]; the pseudo-inverse in the mean-square sense, $\mathbf{Y}^+ = (\mathbf{Y}^{\mathrm{T}}\mathbf{Y})^{-1}\mathbf{Y}^{\mathrm{T}}$ produces highly irregular coefficients. As in the previous section, the difficulty can be solved using a singular value decomposition of Y and truncating the contribution of the least significant singular values.

Numerical simulations have shown that in a system without noise, the rank of the system is equal to the number of modes which respond significantly in the frequency band of interest (assuming this number is smaller that the number n of sensors in the array). When dealing with actual experimental data, the gap in magnitude between significant and insignificant singular values disappears and some trial and error is needed to select the appropriate number of singular values in the truncated expansion.

3. Experiment

Fig. 5 shows a view of the experimental set-up that consists of a 4 mm thick glass plate (0.54 m × 1.24 m) mounted in a standard window frame that is fixed on a concrete box. The sensor array consists of (4 × 8) piezoceramic (PZT) patches (13.75 mm × 25 mm) glued on the plate according to a regular mesh. The set-up and the linear combiner hardware are described in Ref. [6] where they were used in a volume velocity sensor. The resonance frequencies and structural damping of the plate are given Table 1.

Fig. 6 shows the weighting coefficients α_i leading to modal filters for the first four modes of the plate, obtained using Eqs. (15) and (19). One can tailor a FRF similar to Fig. 3 with alternating

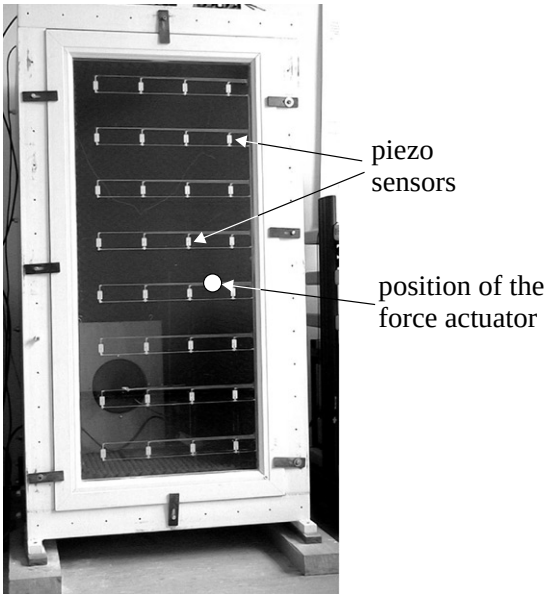

Fig. 5. Experimental set-up: glass plate covered with an array of (4×8) piezoelectric patches.

Table 1
Natural frequencies and structural damping of the plate

Mode	Frequency (Hz)	Damping (%)
(1, 1)	42.5	2.31
(1, 2)	55.9	1.08
(1, 3)	87.1	1.24
(1, 4)	118.7	2.42

poles and zeros and unit amplitudes at the resonances. Fig. 7 shows the FRF measured between the actuator and the sensor output with weighting coefficient given by Eq. (13). An excellent agreement is observed at low frequency, but the measured FRF departs substantially from the expected one at higher frequency.

4. Spatial aliasing

As illustrated in the previous section, reconfigurable sensor arrays work very well as modal filters in a limited frequency band. However, they are subject to spatial aliasing which degrades their behaviour beyond this frequency band by reducing the sensor roll-off. This is again illustrated with the analytical example of Fig. 8. The linear combiner coefficients of the (4×8) PZT array sensor are selected to isolate the first mode. Fig. 8 shows the FRF between four point force actuators acting in phase (same current applied to all) and located as indicated in Fig. 8a,

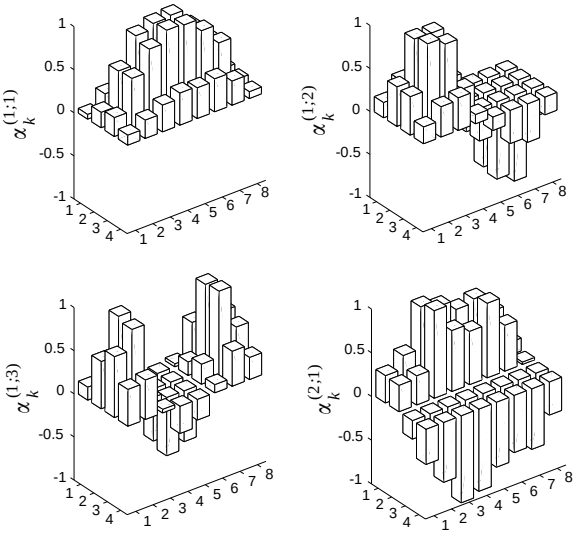

Fig. 6. Weighting coefficients α_i (normalized) leading to modal filters for the first four modes of the plate.

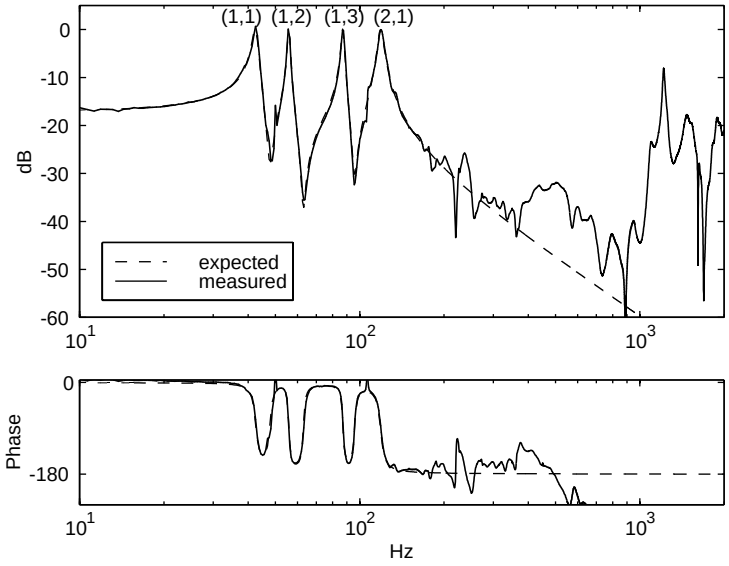

Fig. 7. FRF with prescribed unit amplitude at the resonant peaks, obtained with weighting coefficients $\alpha = \alpha_{(1,1)} + \alpha_{(1,2)} + \alpha_{(1,3)} + \alpha_{(2,1)}$. Comparison between expected and experimental results.

and the linear combiner output. When the sensor is used in an active vibration control system, this reduces the roll-off of the open-loop transfer function, which imposes strong limitations on the bandwidth of the control system (a good sensor should have a bandwidth at least one decade larger than that of the control system).

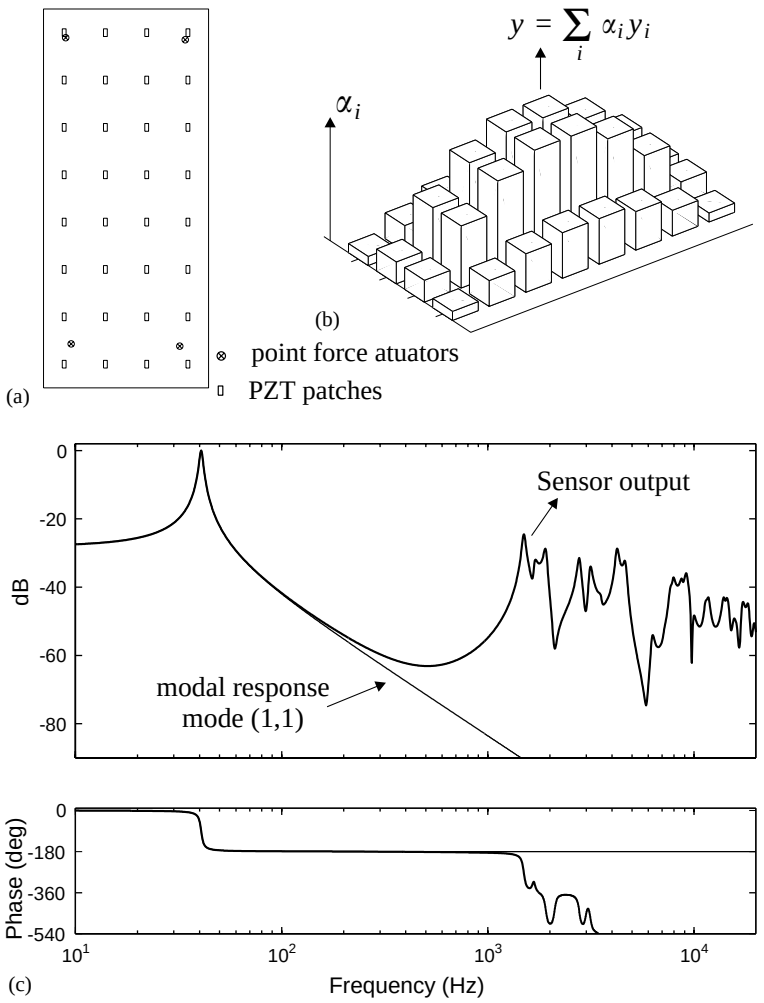

Fig. 8. (a) Geometry of the 4×8 array sensor, (b) weighting coefficients α_i of the linear combiner, (c) comparison of the FRF between the actuators and the modal response of mode (1,1) and the sensor output (numerical simulation).

The spatial aliasing is the counterpart of the better known time aliasing: when the wave number (k) of one mode exceeds the number (n) of sensors regularly spaced in that direction, the sensor output appears as generated by a mode with a lower wave number ($2n - k$). It is illustrated in Fig. 9 for the plate considered previously. The left part of Fig. 9 shows the mode shapes (1,1) and (1,15); the diagrams on the right show the electric charges Q_i generated by these modes on the PZT patches (numerical simulation). The electric charges generated by mode (1,15) at 1494 Hz have the same shape as those generated by mode (1,1). As a result, the orthogonality relationship (4) between the linear combiner coefficients α_i and the sensor modal gains cannot be enforced and the modal sensor designed for mode (1,1) responds to mode (1,15) as well. The limit frequency of

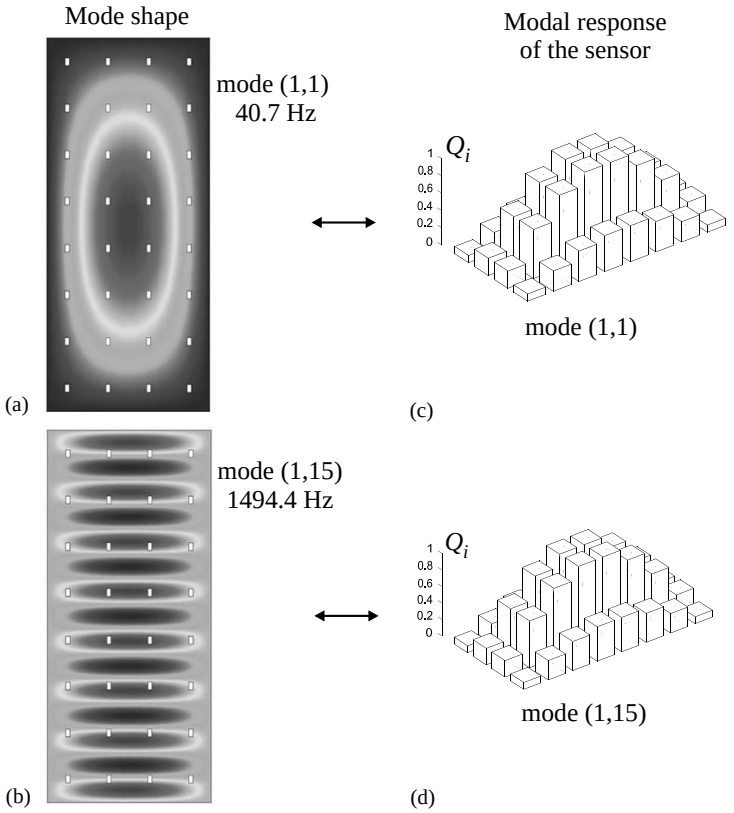

Fig. 9. Spatial aliasing: (a), (b) mode shapes (1,1) and (1,15); (c), (d) electric charges Q_i generated by mode (1,1) and mode (1,15).

the modal filter is given by the natural frequency of the mode with wavenumber equal to the size of the sensor array.

Fig. 10 shows a numerical simulation of the influence of the sensor array on the open-loop FRF of a modal filter for mode (1,1). Because of the high modal density, wide-band modal filtering may require a sensor array of large size which may not be practical because of the independent conditioning electronics, but this is unescapable with discrete array sensors.

5. Distributed sensor

As has been seen in the previous section, the need for distributed sensors arises from the necessity to reduce the spatial aliasing. Although the theory of modal distributed piezoelectric sensors has been known for some time [10,11], they have never been implemented in practice to two-dimensional structure, because the theory is based on tailoring the piezoelectric coefficients, which cannot be done in practice at this time. In this Section, a *practical* way of designing a distributed modal filter is proposed.

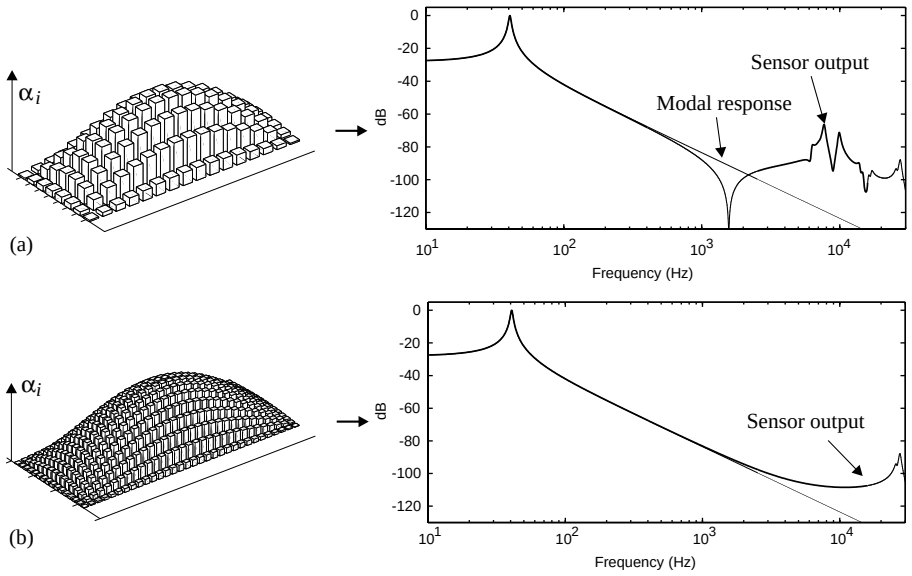

Fig. 10. Effect of the size of the array on the open-loop FRF: (a) (8 × 16), (b) (16 × 32).

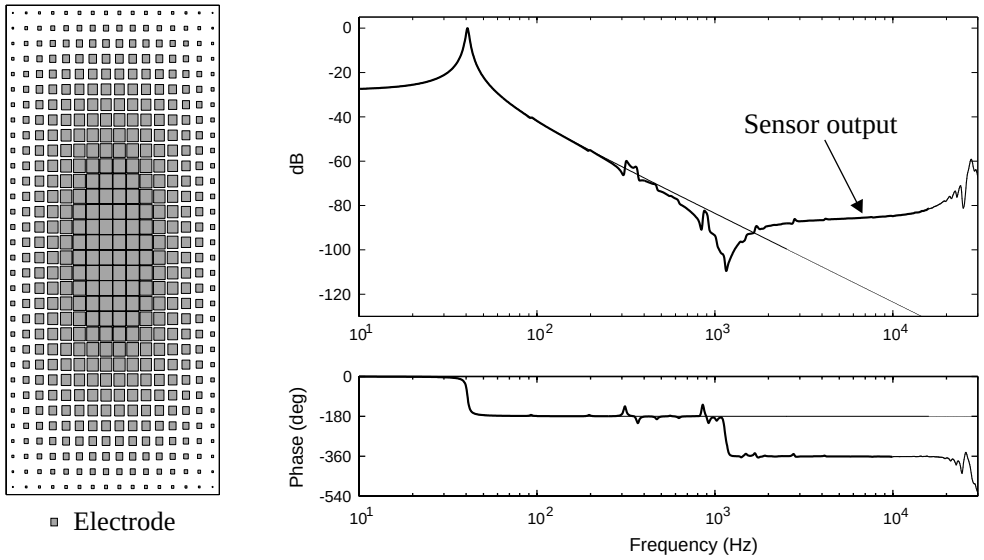

Fig. 11. Variable size array (the (16 × 32) patches are interconnected).

The theory of modal filtering with distributed sensors can be addressed in two different ways: (i) based on the orthogonality relationships for distributed structures or (ii) as a limit case of a discrete array filter when the number of elements in the array increases to infinity. The first approach was addressed by Lee and Moon [11]; the second one which is more intuitive in view of the previous discussion on spatial aliasing will be considered here.

As illustrated in Fig. 10, the bandwidth of an array sensor can be increased by increasing the number of sensing elements in the array. In the example of Fig. 10b, the sensor bandwidth is close to 5000 Hz with a sensor array containing 16×32 elements. However, the number of independent conditioning electronic units becomes rapidly prohibitive.

If the weighting coefficients α_i are known before hand and if we give up the programmability of the linear combiner, the coefficients α_i can be embedded in the individual sensing elements. This is illustrated in Fig. 11; the area of the individual piezoelectric patches (more precisely the electrode area) is taken to be proportional to the corresponding coefficient α_i in the linear combiner. The various electrodes of the sensor array are connected together and the total electric charge generated on the array is proportional to the output of the linear combiner. This configuration can be easily manufactured with a segmented electrode etched on a continuous PVDF layer using classical lithography techniques; it requires only a single amplifier, but the weighting coefficients cannot be changed on-line as in the linear combiner. The modal filtering property of this concept is illustrated in Fig. 11; spatial aliasing still occurs beyond 2000 Hz and it can be pushed even further by increasing the number of segments in the electrode.

6. A new electrode concept

The distributed sensor can be viewed as the limit discrete array sensor where the number of sensing elements increases and the electrode density is such that the local production of electric charges matches the desired local effective weighting coefficient. A practical way to achieve this is to use a "porous" electrode as shown in Fig. 12; the maximum sensitivity is obtained where the electrode is continuous (in the centre in Fig. 12a) and the local sensitivity is decreased continuously by introducing some porosity in the continuous electrode by means of a honeycomb design (Fig. 12b). The local electrode density is selected in such a way that the local production of electric charges matches the desired local weighting coefficient $\alpha(x, y)$.

Consider a piezoelectric film polarized in the direction normal to its plane and covered with electrodes Ω as in Fig. 13. According to the two-dimensional theory of piezoelectric films, if a sample is subject to a plane strain field aligned on the orthotropy axes of the material, and if the electrodes are connected to a charge amplifier which cancels the electric field across the piezoelectric film, the electric charge produced on the electrodes is

$$Q = \int_{\Omega} (e_{31} S_1 + e_{32} S_2)\, \mathrm{d}\Omega, \tag{20}$$

where S_1 and S_2 are the strain components along the orthotropy axes in the mid-plane of the film, and e_{31} and e_{32} are the piezoelectric constants of the material. The integral extends over the area of the electrode, or more precisely, the area Ω over which the two electrodes overlap, where the electrical field is zero. According to Eq. (20) changing the local electrode density ($\mathrm{d}\Omega$) is equivalent to changing the piezoelectric coefficients e_{31} and e_{32} in the same ratio. Since Ω refers to the area where the two electrodes overlap, the motif may be etched on the electrodes on both sides of the piezo film (Fig. 12c) or only on one side, with a continuous electrode on the other side (Fig. 12d), which seems technologically simpler, because the two electrodes do not have to be aligned precisely on top of each other.

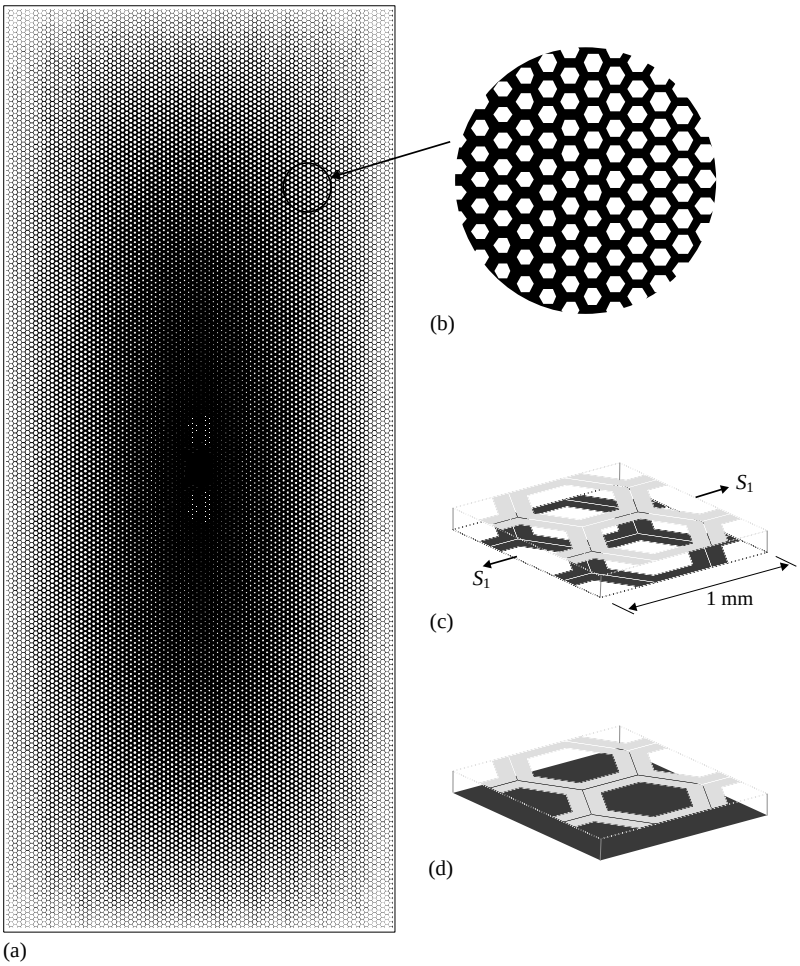

Fig. 12. (a) Porous electrode, (b) detail of the motif with variable porosity, (c) double sided motif (fraction of electrode area = 50%), (d) single sided motif (the other electrode is continuous).

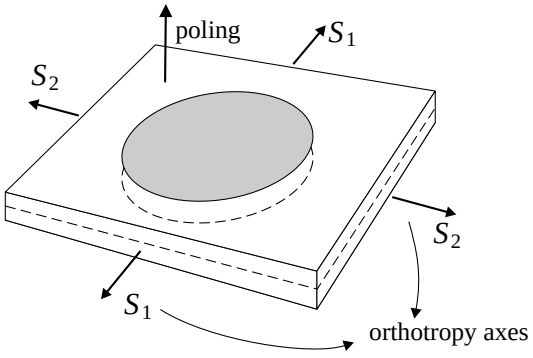

Fig. 13. Sample of piezoelectric film polarized in the direction normal to its plane.

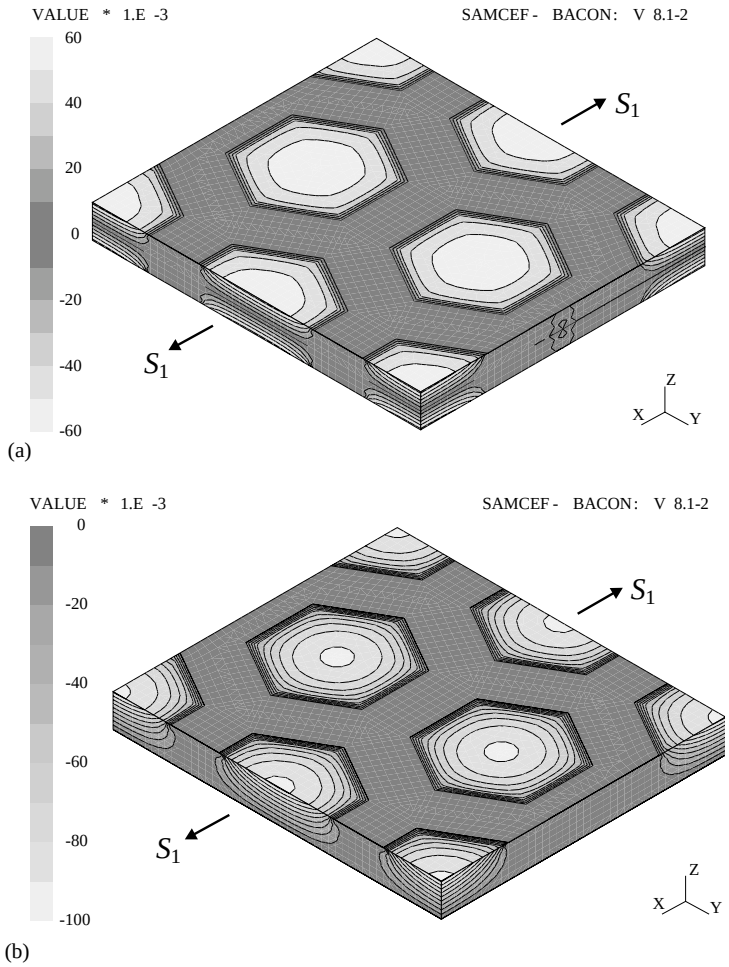

Fig. 14. Tridimensional finite element analysis. Isopotential surfaces. (a) Two-sided electrode. (b) One-sided electrode.

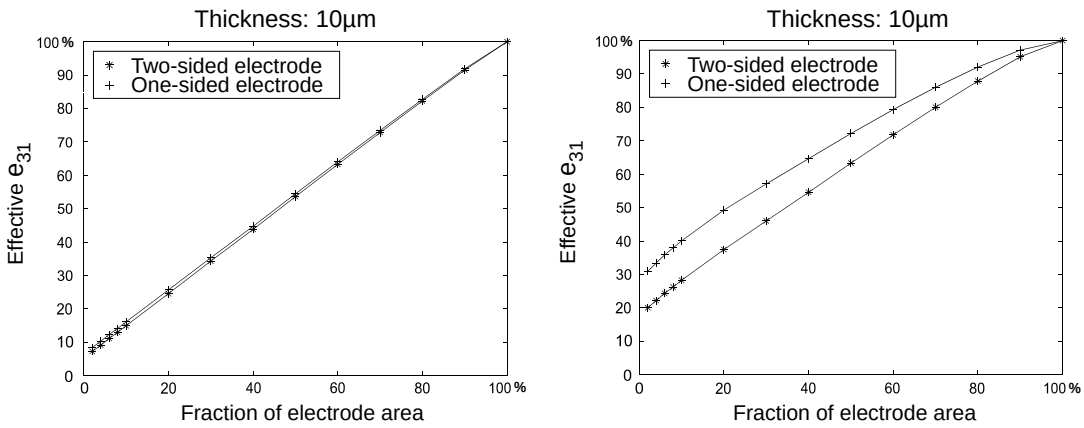

Fig. 15. Effective piezoelectric coefficient versus fraction of electrode area.

Eq. (20) assumes that the size of the electrode is much larger than its thickness. However, when the motif of the electrode becomes small, tridimensional (edge) effects start to appear and the relationship between the porosity and the equivalent piezoelectric property is no longer linear.

The exact relationship between the porosity and the equivalent piezoelectric coefficients can be explored with a tridimensional finite element analysis software [22]. Fig. 14 shows the isopotential surfaces for the two electrode configurations when a small sample (1 mm × 1 mm × 100 μm) is subjected to a strain along the x-axis and a potential difference $V = 0$ is enforced between the electrodes; the material assumed in this study is isotropic PVDF (copolymer) polarized in the direction perpendicular to the electrodes. The edge effects appear clearly in the figures. For this sample, Fig. 15 shows the relationship between the effective piezoelectric coefficient and the fraction of electrode area; the two electrode configurations are considered for two sample

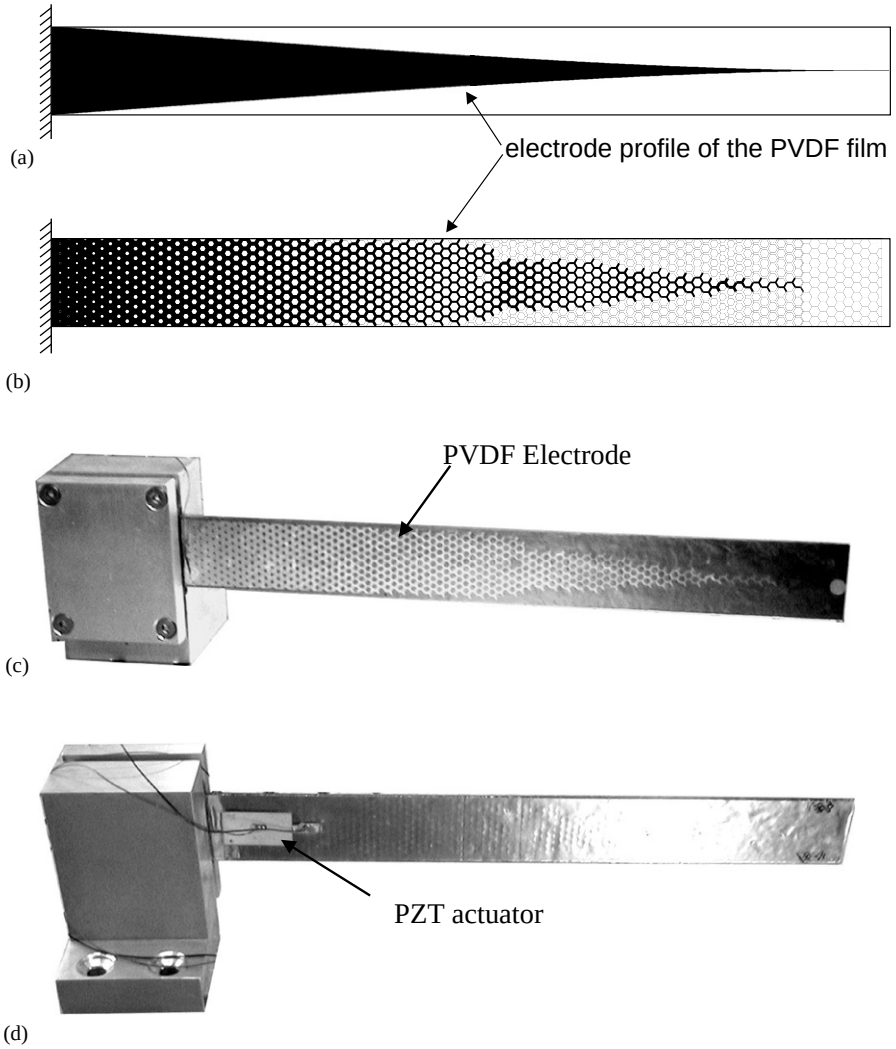

Fig. 16. Experimental set-up for the honeycomb electrode validation.

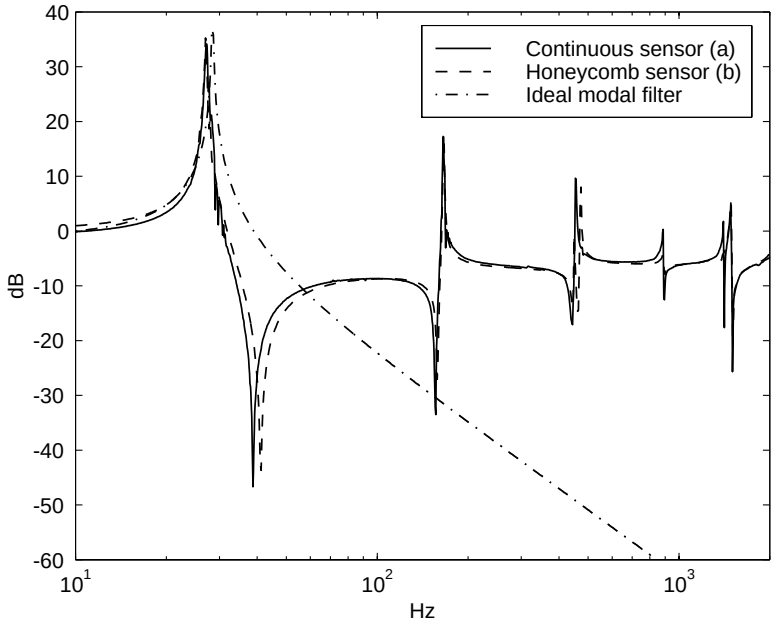

Fig. 17. Comparison between the measured FRF of the continuous and honeycomb sensors with the FRF of the analytical beam model.

thicknesses (10 μm × 100 μm); it is seen that for a very thin sensor, the two electrode configurations produce the same results and the relationship is almost linear.

7. Validation test

To the author's knowledge, this concept of "porous" electrode is new [23]. This section reports on the preliminary test program aiming at validating the new concept.

Fig. 16 shows the experimental set-up. Two cantilever beams made of glass of 240 mm × 27 mm × 1.83 mm are equipped on one side with a PZT actuator and on the opposite side with an isotropic PVDF (copolymer) sensor with a shaped electrode. In one case, the electrode profile matches the modal filter of the beam theory [10]; in the other case, the same axial variation of the piezoelectric properties is achieved with the porous design described in the previous section. However, to guarantee the continuity of the honeycomb electrode during the manufacturing process, the width of the electrode is constrained to be larger than 0.5 mm; this explains why the electrode design is tapered near the free end of the sample.

Fig. 17 compares the FRF between the PZT actuator and the PVDF sensor for the two electrode designs. The two curves are remarkably close, although significantly different from the ideal modal filter; this difference is partly due to the fact that the PVDF material is isotropic ($e_{31} = e_{32}$). These experimental results also agree well with finite element calculations (Mindlin shell [22]) for the continuous electrode sensor (Fig. 18).

Further tests are under way to validate the new electrode design on rectangular plates.

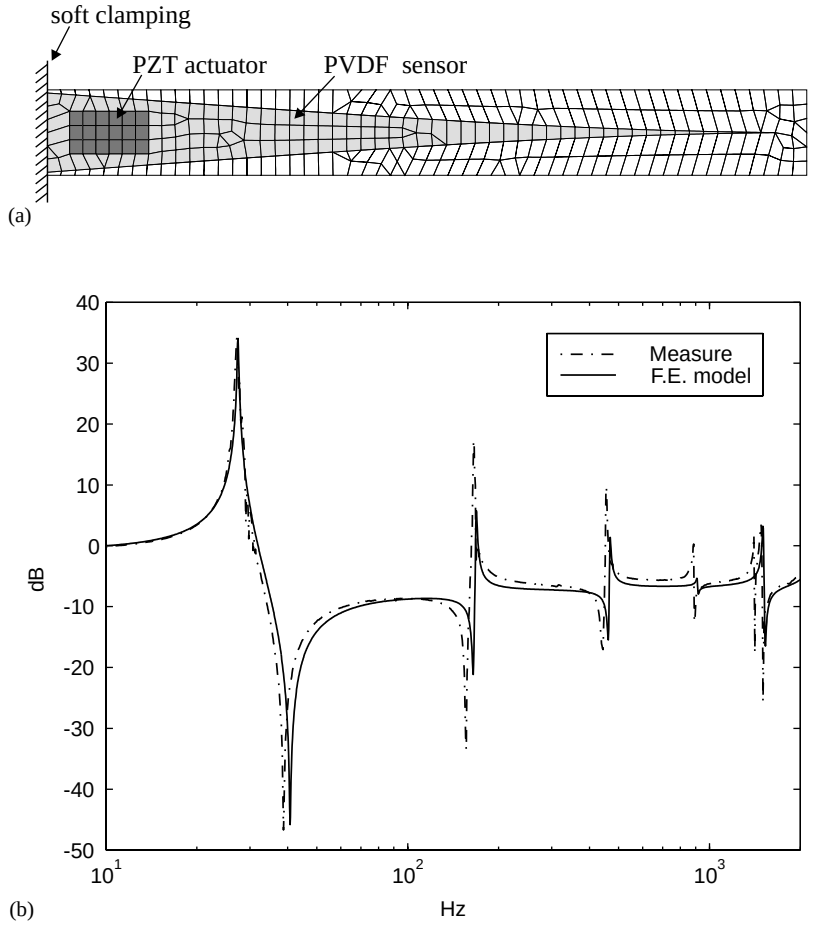

Fig. 18. (a) Finite element model of the beam with its piezoelectric modal sensor, (b) and comparison between the finite element and the experimental results (continuous sensor).

8. Conclusions

This paper examines the construction of modal filters with discrete array sensors and with continuous distributed PVDF films. The lack of roll-off of discrete array sensors due to spatial aliasing has been discussed. A new porous distributed electrode concept has been introduced which allows the effective piezoelectric coefficients to be tailored in two dimensions and eliminates the spatial aliasing. Preliminary validation tests of the porous electrode design have been presented on a cantilever beam.

Acknowledgements

This work was supported by the Ministry of *Région Wallonne* (DGTRE) under Grant No. 014427 (SAAB) and the Inter University Attraction Pole IUAP 5 on Advanced Mechatronic Systems.

References

[1] L. Meirovitch, H. Baruh, The implementation of modal filters for control of structures, American Institute of Aeronautics and Astronautics Journal of Guidance 8 (6) (1985) 707–716.
[2] Q. Zhang, R.J. Allemang, D.L. Brown, Modal filter: concept and applications, International Modal Analysis Conference, 1990, pp. 487–496.
[3] S.J. Shelley, K.L. Lee, T. Aksel, A.E. Aktan, Active control and forced-vibration studies on highway bridge, Journal of Structural Engineering 121 (1995) 1306–1312.
[4] N. Tanaka, Y. Kikushima, Active modal control and its robustness using point sensors and point actuators, JSME International Journal, Series C 42 (1) (1999) 54–61.
[5] H. Sumali, K. Meissner, H.H. Cudney, A piezoelectric array for sensing vibration modal coordinates, Sensors and Actuators A 93 (2001) 123–131.
[6] A. François, P. De Man, A. Preumont, Piezoelectric array sensing of volume displacement: a hardware demonstration, Journal of Sound and Vibration 244 (3) (2001) 395–405.
[7] S.A. Collins, D.W. Miller, A.H. Von Flotow, Distributed sensors as spatial filters in active structural control, Journal of Sound and Vibration 173 (4) (1994) 471–501.
[8] D.K. Miu, Mechatronics: Electromechanics and Contromechanics, Springer, New York, 1993.
[9] S.E. Burke, J.E. Hubbard, Active vibration control of a simply supported beam using a spatially distributed actuator, IEEE Control Systems Magazine, August 1987, pp. 25–30.
[10] C.K. Lee, Theory of laminated piezoelectric plates for the design of distributed sensors/actuators. Part i: governing equations and reciprocal relationships, Journal of Acoustical Society of America 87 (3) (1990) 1144–1158.
[11] C.K. Lee, F.C. Moon, Modal sensors/actuators, Journal of Applied Mechanics 57 (1990) 434–441.
[12] Y. Gu, R.L. Clark, C.R. Fuller, A.C. Zander, Experiments on active control of plate vibration using piezoelectric actuators and polyvinylidene fluoride (pvdf) modal sensor, Journal of Vibration and Acoustics 116 (1994) 303–308.
[13] R.L. Clark, S.E. Burke, Practical limitations in achieving shaped modal sensors with induced strain materials, Journal of Vibration and Acoustics 118 (1996) 668–675.
[14] F. Charette, A. Berry, Active control of sound radiation from a plate using a polyvinylidene floride volume displacement sensor, Journal of Acoustical Society of America 103 (3) (1998) 1493–1503.
[15] N. Tanaka, S.D. Snyder, C.H. Hansen, Distributed parameter modal filtering using smart sensors, Journal of Vibration and Acoustics 118 (1996) 630–640.
[16] J. Rex, S.J. Elliott, The QWSIS—a new sensor for structural radiation control, in: MOVIC, Yokohama, September 1992, pp. 339–343.
[17] J. Kim, J.-S. Hwang, S.J. Kim, Design of modal transducers by optimizing spatial distribution of discrete gain weights, American Institute of Aeronautics and Astronautics Journal 39 (10) (2001) 1969–1976.
[18] S.E. Miller, Y. Oshman, H. Abramovich, Modal control of piezolaminated anisotropic rectangular plates, Part 1: modal transducer theory, American Institute of Aeronautics and Astronautics Journal 34 (9) (1996) 1868–1875.
[19] W.K. Gawronski, Dynamics and Control of Structures, a Modal Approach, Springer, Berlin, 1998.
[20] G. Strang, Linear Algebra and its Applications, 3rd Edition, Harcourt Brace Jovanovich, New York, 1988.
[21] G.D. Martin, On the Control of Flexible Mechanical Systems, Ph.D. Thesis, Stanford University, 1978.
[22] V. Piefort, Finite Element Modeling of Piezoelectric Active Structures, Ph.D. Thesis, Université Libre de Bruxelles, 2001.
[23] A. Preumont, Method for Shaping Laminar Piezoelectric Actuators and Sensors and Related Devices, March 2002, International patent application PCT/BE02/00026.